

SUPPORTING INFORMATION

Methods

Theoretical models

To attain high energy-conversion efficiency, the excited electron and hole pairs should dissociate into separate positive and negative charges to escape from recombination due to the coulombic attraction. To achieve this process, the binding energy must be overcome. That is, the dye molecule should possess less exciton binding energy for high-energy conversion. Here, the exciton binding energy was calculated using the formula[1,2]:

$$E_b = IP - EA - E_{opt\ gap} \quad (1)$$

$$IP = -E_{HOMO} \quad (2)$$

$$EA = -E_{LUMO} \quad (3)$$

where IP is ionization energy, EA is electron affinity energy and $E_{opt\ gap}$ is the excitation energy.

To understand the influencing factors of J_{SC} , one calculated the time of electron injection. The charge separation process of the sensitizer can be estimated by the Newns-Anderson model[3]. When the excited state adsorbate interacts with the energy band of a semicontinuous base semiconductor (TiO_2), its energy obeys the following Lorentzian distribution[4]:

$$L_{LUMO}(E) = \frac{1}{\pi} \frac{\left(\frac{\hbar\Gamma}{2}\right)}{(E - E_{LUMO(ads)})^2 + \left(\frac{\hbar\Gamma}{2}\right)^2} \quad (4)$$

The broadening width $\hbar\Gamma$ is derived from the mean deviation of the LUMO (adsorbate) levels, which is evaluated as follows[5]:

$$\hbar\Gamma = \sum_i p_i |\varepsilon_i - E_{LUMO(ads)}| \quad (5)$$

The $E_{LUMO(ads)}$ of dye's LUMO level after adsorption in eq 12 is characterized by

$$E_{LUMO(ads)} = \sum_i p_i \varepsilon_i \quad (6)$$

$$p_i = \frac{\sum_{i \in ads} (c_{ij}^A)^2}{\sum_{i \in ads@TiO_2} (c_{ij}^A)^2} \quad (7)$$

where p_i is the percentage (%) of the electron distribution on the adsorbate in the i -th non-occupied molecular orbital of the dye molecule; ε_i is the energy level (eV) of the i -th non-occupied molecular orbital of the dye molecule. Therefore, the photogenerated electron injection time can be calculated by the following formula:

$$\tau(fs) = \frac{658}{\hbar\Gamma} \quad (8)$$

To further estimate J_{SC} , one calculated the lifetime (τ_1) of the first excited state (S_1). Value of τ_1 is one of the important factors affecting the efficiency of electron transfer [6], which can be expressed by the following formula[7,8]:

$$\tau_1 = \frac{1.499}{f_1 \cdot E^2} \quad (9)$$

where E is the excitation energy of the first excited state (cm^{-1}) and f_1 is the oscillator strength.

At the same time, the fluorescence lifetime (τ_2) is an important factor affecting charge recombination[9]:

$$\tau_2 = \frac{a \cdot c^3 \cdot u^2}{2 \cdot f_2 \cdot e_2^2} \quad (10)$$

where c is the speed of light, f_2 is the oscillator strength in the fluorescence state, and e_2 is the fluorescence energy.

To quantitatively describe the molecular TIC process, one calculated the parameters D_{CT} , S_r , Δr , and E_c for the dye@ TiO_2 model; these parameters can be obtained from the following formula[10–12]:

$$D_{CT} = \sqrt{|X_e - X_h|^2 + |Y_e - Y_h|^2 + |Z_e - Z_h|^2} \quad (11)$$

$$S_r = \int S_r d(r) = \int \sqrt{\rho_{(r)}^{hole} \rho_{(r)}^{ele}} d(r) \quad (12)$$

$$\Delta r = \frac{\sum_{ij} (K_i^j)^2 [\langle \varphi_j | r | \varphi_j \rangle - \langle \varphi_i | r | \varphi_i \rangle]}{\sum_{ij} (K_i^j)^2} \quad (13)$$

$$E_c = \frac{e^2}{4\pi\epsilon_0\epsilon_r} \iint \frac{\rho_h(\vec{r}_1)\rho_e(\vec{r}_2)}{|\vec{r}_1 - \vec{r}_2|} d^3\vec{r}_1 d^3\vec{r}_2 \quad (14)$$

where D_{CT} is the charge transferred distance between hole and electron centroids; X , Y , and Z represent three-dimensional directions. X_e and X_h represent the density of charges at a specific orientation, such as $X_e = \int x\rho_e(r)dr$ for electrons and $X_h = \int x\rho_h(r)dr$ for holes, respectively. The S_r index characterizes the overlap extent of the hole and electron, where $\rho_{(r)}^{hole}$ and $\rho_{(r)}^{ele}$ are the density distributions of holes and electrons. Δr represents the length of charge transfer during electronic excitation. E_c is the Coulomb attraction, e and ϵ_0 are the elementary charge and vacuum dielectric constant, respectively.

In addition, the power conversion efficiency (η) of solar cell is quantified using the following formula:

$$PCE = \frac{V_{oc}J_{SC}FF}{P_{inc}} \quad (15)$$

Where V_{oc} is the open-circuit voltage, J_{SC} is the short-circuit current density, FF is the fill factor, and P_{inc} is the input power of incident solar light (taking the measurement value of 100 mW cm^{-2}).

In general, J_{SC} largely depends on the light-harvesting ability including the optical absorption region and intensity of the dye, which can be evaluated using the following equation[13–18]:

$$J_{SC} = e \int \frac{I_S(\lambda)}{E(\lambda)} LHE(\lambda) \phi_{inj} \eta_{coll} d\lambda \quad (16)$$

where e is defined as unit charge; $LHE(\lambda)$ represents the light absorption efficiency; ϕ_{inj} and η_{coll} present electron injection and collection efficiency; and $I_S(\lambda)$ is the photon flux under AM1.5 G solar spectrum irradiation; $E(\lambda)$ is the energy of a single photon with wavelength λ , calculated by $1240/\lambda \text{ (m)}$ [19]. The definition of $LHE(\lambda)$ is the following[20–23]:

$$LHE(\lambda) = 1 - 10^{-\Gamma\sigma(\lambda)} \quad (17)$$

$$\sigma(\lambda) = \varepsilon(\lambda) \times 10^3 \quad (18)$$

where Γ is the molecular adsorption value on the surface of the semiconductor ($mol \cdot cm^{-2}$), and according to the experimental reference, all molecular adsorption values based on R of $5.2 \times 10^{-8} mol/cm^2$ where used as a reference; $\sigma(\lambda)$ stands for molecular absorption cross-section ($cm^2 \cdot mol^{-1}$) and $\varepsilon(\lambda)$ is the molar absorption coefficient [24,25]. The electron injection and electron composited efficiency can be determined as[25]:

$$\phi_{inj} = \frac{1}{1 + \frac{\tau_{inj}}{\tau_{relax}}} \quad (19)$$

$$\eta_{coll} = \frac{1}{1 + \frac{\tau_{trans}}{\tau_{rec}}} \quad (20)$$

Where τ_{inj} is the required electron injection time of the dye to the TiO₂ surface based on Marcus' theory[10,25], and τ_{relax} is the relaxation lifetime from the experiment (10 ps)[10,25,26]; τ_{trans} is the electron transfer time from TiO₂ to the redox couple (5 ps)[25], and τ_{rec} is the attenuation time. Based on the Marcus theory, all investigated molecules have relative longer recombination time, and the obtained all molecular η_{coll} is tending to 1.

According to Marcus' theory, the injection time τ_{inj} and the electron injection rate K_{inject} is given by the following two relations[27,28]:

$$\tau_{inj} = \frac{10^{12}}{K_{inject}} \quad (21)$$

$$K_{inject} = \sqrt{\frac{\pi}{\hbar^2 \lambda_{tot} K_B T}} \exp\left(\frac{-\beta r_{inj}}{A}\right) \exp\left[\frac{-(-\Delta G^\circ + \lambda_{tot})^2}{4\lambda K_B T}\right] \quad (22)$$

where ΔG° is the driving force for the reaction of electrons injection; λ_{tot} is the total recombination energy; r_{inj} is the distance between the cyanoacrylic acid and the surface of TiO₂; \hbar is the Planck constant, β is the attenuation parameter (0.7)[10,25]; A is a fixed value [25], and $K_B T$ is thermal energy (0.025852 eV). The parameters are obtained using the following equations :

$$\Delta G^\circ = E_{LUMO} - E_{CBM} \quad (23)$$

$$\lambda_{tot} = [E_0^+ - E_+^+] + [E_+^0 - E_0] + [E_0^- - E_-^-] + [E_-^0 - E_0] \quad (24)$$

where E_{LUMO} is the *LUMO* energy of the dye, and E_{CBM} is the simulated conduction band minimum of titanium dioxide, and E_0 is the neutral molecule's energy in the ground state, and E_0^+/E_0^- is the cation (anion)'s energy with the geometry of the neutral molecule, and E_+^+/E_-^- is the energy of the cationic (anionic) optimized under the cationic (anionic) structure, and E_+^0/E_-^0 is the neutral's energy with the geometry of the cationic (anionic) state.

The V_{oc} is determined by the difference between the quasi-Fermi level of the semiconductor (E_{F, TiO_2}) and the redox potential of the redox couple (E_{redox})[18].

The V_{oc} can be obtained by the following formula[23,29–33]:

$$V_{oc} = E_{F, TiO_2} - E_{redox} = \frac{1}{e} \left[E_{CB} + \Delta E_{CB} - E_{redox} + K_B T \ln \left(\frac{n_c}{N_{CB}} \right) \right] \quad (25)$$

$$\Delta E_{CB} = \frac{-e\mu_{normal}\gamma}{\varepsilon\varepsilon'} \quad (26)$$

Where e is the unit charge, E_{CB} is the conduction band energy level of the semiconductor (–4.0 eV), ΔE_{CB} is the displacement of the energy level of the conduction band[28,32,33], E_{redox} is the electrolyte (I^-/I_3^-) level (–4.8 eV), $K_B T$ is thermal energy (0.025852 eV), n_c is the electron number in the conduction band [25,31], N_{CB} is the electron density of state ($7 \times 10^{20} \text{ cm}^{-3}$)[10,25,31]; ε and ε' are the dielectric constant of the organic monolayer and the dielectric constant of the vacuum, respectively; μ_{normal} is the dipole moment component perpendicular to the direction of TiO_2 surface; and γ is the concentration of surface. ΔE_{CB} can be calculated by the difference between the intersections of the TiO_2 PDOS and pure TiO_2 DOS lines on the energy axis[34,35].

According to the current density-voltage properties of solar cells, the I-V curve can be depicted in the presence of known JSC and V_{oc} [10,17,18,25,25,36,37]:

$$I = J_{sc} - I_S \left(\exp \left(\frac{eV}{K_B T} \right) - 1 \right) \quad (27)$$

$$I_S = \frac{J_{sc}}{\exp(eV_{oc}/K_B T) - 1} \quad (28)$$

$$FF = \frac{I_m V_m}{J_{SC} V_{oc}} \quad (29)$$

Where I is current; V is photovoltage; I_s is the reverse saturation current[10,25]; $I_m V_m$ is the maximum power[10,15,25], and FF is the fill factor[10,25,38].

Table S1. Calculated maximum absorption wavelengths (λ_{max}/nm), vertical excitation energy (E), oscillator strengths (f), light-harvesting efficiency (LHE), and main transition configuration of the isolated dyes in dichloromethane solution under TD-BHandH/6-31G(d,p) level.

Dyes	$\lambda_{max}(nm)$	$E_{\lambda_{max}}$ (eV)	f	LHE	Major contribs*
<i>R_d</i>	513.00	2.417	1.4216	0.962	H-2→L (41%), H→L (53%)
<i>Tat-1</i>	538.43	2.3027	1.7729	0.983	H-2→L (47%), H→L (41%)
<i>Tat-2</i>	594.88	2.8337	1.5780	0.974	H-2→L (44%), H→L (46%)
<i>Tat-3</i>	502.20	2.4688	2.2094	0.994	H-2→L (45%), H→L (39%)

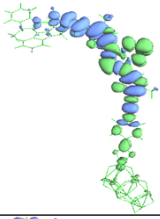
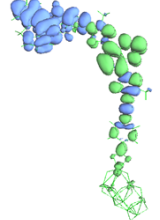
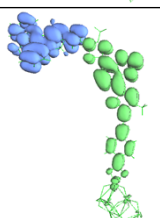
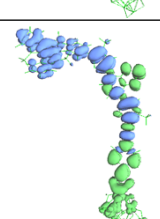
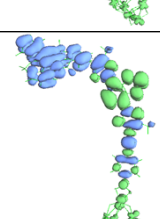
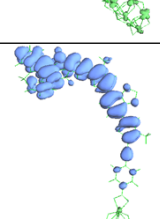
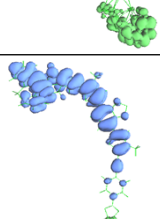
Tat-4	547.87	2.2630	1.8473	0.986	H-2→L (49%), H→L (39%)
Tat-5	559.13	2.9173	1.5809	0.974	H-2→L (46%), H→L (44%)
Tat-6	648.89	1.9107	1.1906	0.963	H-2→L (43%), H→L (48%)

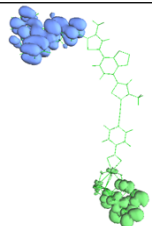
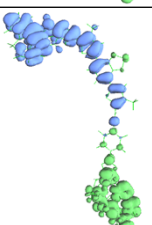
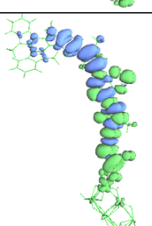
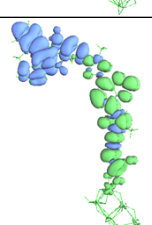
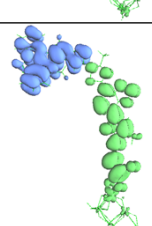
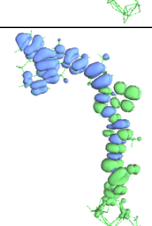
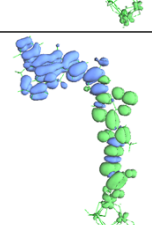
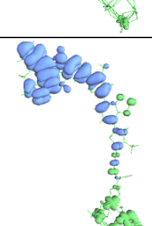
*H: HOMO; L: LUMO.

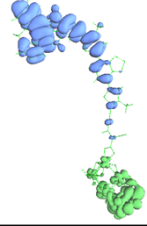
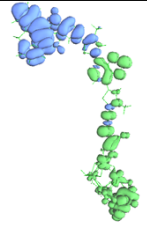
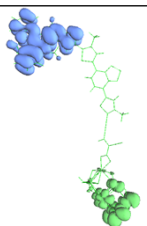
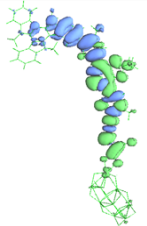
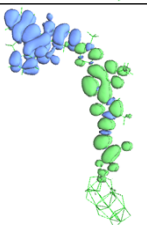
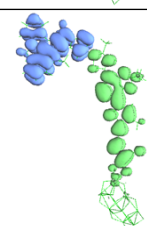
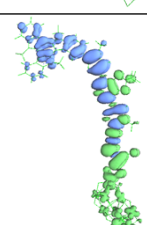
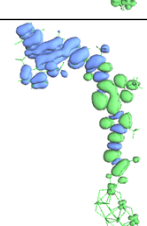
Table S2. Calculated transition properties and excited state lifetime of all dyes

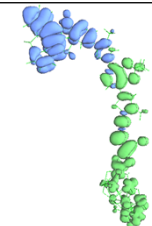
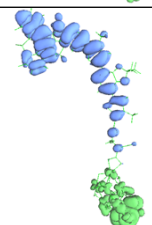
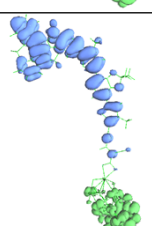
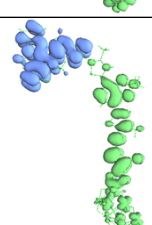
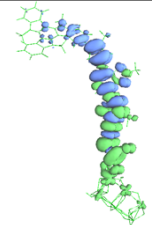
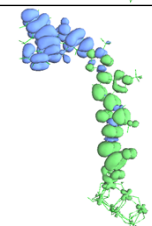
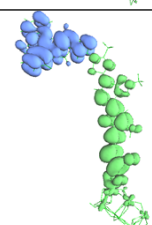
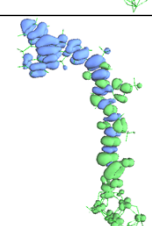
Dyes	E(eV)	Strength f	τ_2 (ns)
R _d	1.9598	1.4592	4.12
Tat-1	1.8675	1.9526	3.39
Tat-2	1.6331	1.5830	5.47
Tat-3	2.0303	2.4572	2.28
Tat-4	1.8361	2.1011	3.25
Tat-5	1.8110	1.6936	4.16
Tat-6	1.3809	0.9698	12.48

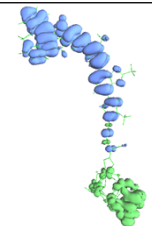
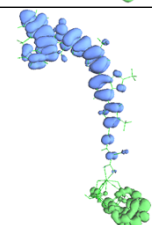
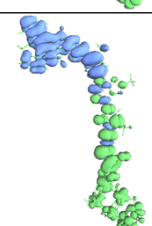
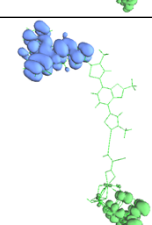
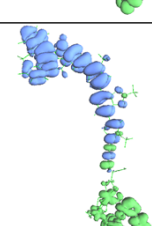
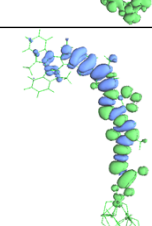
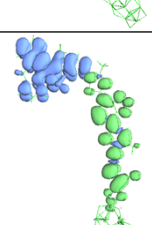
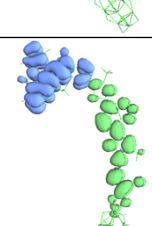
Table S3. Computed charge density difference (CDD) diagram, charge transferred distance between hole and electron centroids (D_{CT}), extent of overlap between hole and electron centroids (Sr), the length of charge transfer during electronic excitation (Δr), and attracting hole-electron coulomb energy (E_c) for the low-lying excited states of each dye.

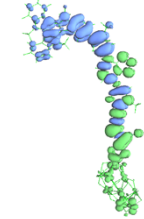
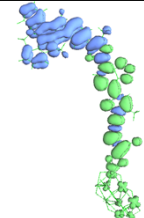
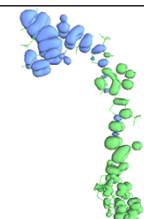
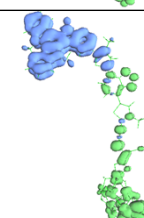
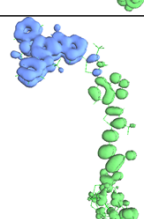
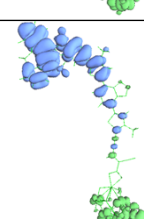
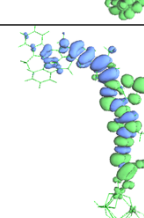
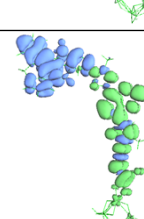
Systems	Transition	Charge-spectra	$D_{CT}(\text{Å})$	$Sr(a.u.)$	$\Delta r(\text{Å})$	$E_c(\text{eV})$
$R_d@(TiO_2)_9$	S0→S1		3.388	0.644	7.109	2.544
	S0→S2		9.982	0.357	6.872	1.496
	S0→S3		13.523	0.075	12.030	1.077
	S0→S4		9.607	0.426	16.019	1.138
	S0→S6		8.037	0.387	7.757	1.259
	S0→S7		26.768	0.020	26.758	0.559
	S0→S8		26.822	0.012	26.937	0.562

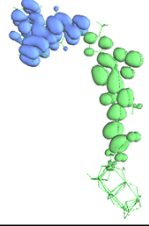
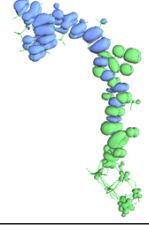
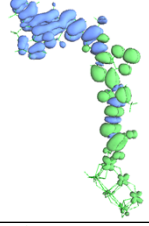
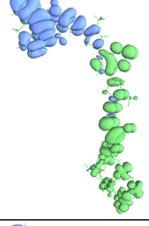
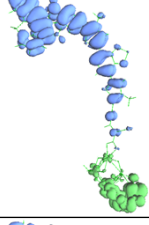
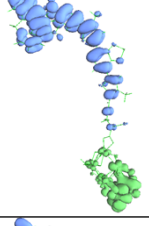
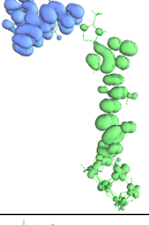
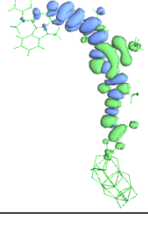
	S0→S9		30.154	0.001	28.766	0.499
	S0→S10		24.789	0.088	23.733	0.472
Tat-1@ (TiO ₂) ₉	S0→S1		5.320	0.4583	9.544	2.213
	S0→S2		10.732	0.404	10.872	1.535
	S0→S3		15.268	0.057	14.091	0.919
	S0→S4		8.753	0.505	14.410	1.624
	S0→S5		8.876	0.451	10.277	1.521
	S0→S7		25.993	0.084	25.662	0.481

	S0→S8		27.504	0.039	26.662	0.467
	S0→S9		21.554	0.157	21.691	0.674
	S0→S10		29.342	0.00044	28.030	0.507
Tat-2@ (TiO ₂) ₉	S0→S1		4.655	0.628	8.892	2.436
	S0→S2		11.997	0.353	9.181	1.420
	S0→S3		13.847	0.172	12.712	1.145
	S0→S4		8.511	0.468	15.087	1.368
	S0→S5		7.876	0.452	8.900	1.571

	S0→S7		18.050	0.224	18.846	0.771
	S0→S8		25.678	0.054	24.714	0.563
	S0→S9		26.087	0.037	24.689	0.537
	S0→S10		18.380	0.037	21.292	0.780
Tat-3@ (TiO ₂) ₉	S0→S1		5.690	0.568	11.244	2.247
	S0→S2		13.695	0.339	12.522	1.253
	S0→S3		17.136	0.046	16.076	0.866
	S0→S4		13.749	0.468	13.936	1.177

	S0→S6		25.984	0.060	26.834	0.516
	S0→S7		26.588	0.010	26.834	0.539
	S0→S8		15.783	0.318	15.450	0.913
	S0→S9		29.898	0.001	28.579	0.500
	S0→S10		22.82	0.143	23.132	0.595
Tat-4@ (TiO ₂) ₉	S0→S1		4.978	0.612	9.127	2.363
	S0→S2		12.801	0.320	11.124	1.328
	S0→S3		13.877	0.227	12.444	1.141

	S0→S4		7.884	0.513	15.273	1.533
	S0→S5		9.693	0.435	10.324	1.384
	S0→S7		19.581	0.170	20.959	0.613
	S0→S8		24.986	0.108	25.234	0.555
	S0→S9		20.886	0.117	23.539	0.730
	S0→S10		27.835	0.048	26.065	0.491
	S0→S1		4.379	0.625	9.190	2.434
	S0→S2		10.363	0.400	10.249	1.503

Tat-5@ (TiO ₂) ₉	S0→S3		14.177	0.064	13.677	1.024
	S0→S4		9.354	0.469	14.887	1.481
	S0→S5		8.984	0.411	9.084	1.364
	S0→S7		18.242	0.177	19.145	0.745
	S0→S8		26.757	0.014	26.500	0.572
	S0→S9		26.450	0.042	24.919	0.508
	S0→S10		17.415	0.033	21.183	0.910
	Tat-6@ (TiO ₂) ₉	S0→S1		4.033	0.626	7.837

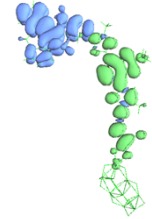
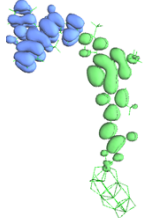
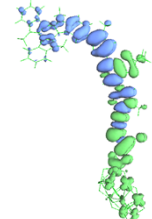
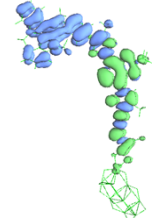
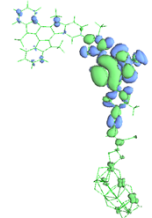
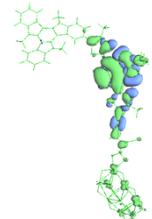
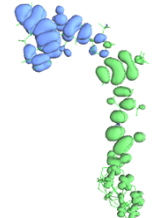
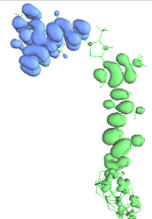
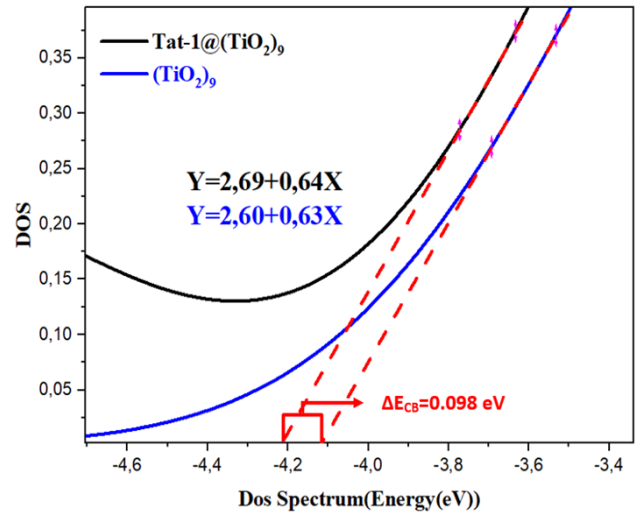
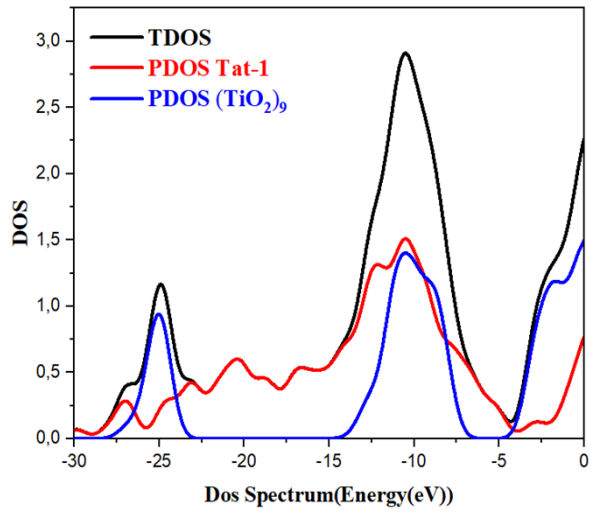
S0→S2		12.455	0.294	8.219	1.310
S0→S3		13.091	0.172	11.785	1.246
S0→S4		7.734	0.476	16.862	1.623
S0→S5		6.678	0.463	7.161	1.622
S0→S6		2.539	0.506	5.606	2.579
S0→S7		3.189	0.414	6.324	2.642
S0→S8		16.861	0.163	17.800	0.749
S0→S10		17.636	0.026	21.488	0.899

Table S4. The calculated driving force for electrons injection and reorganization energies. (in eV).

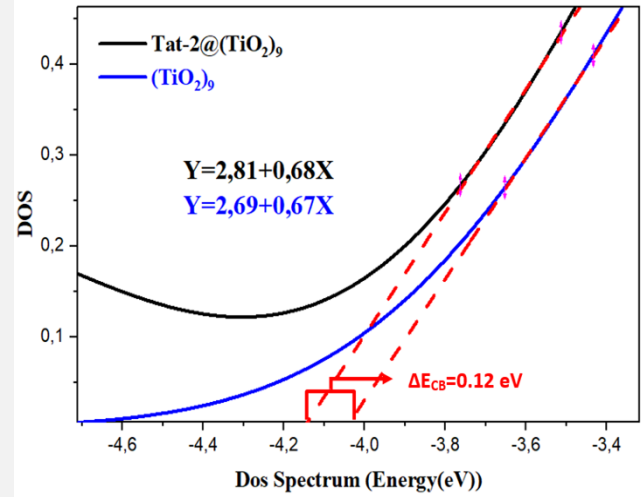
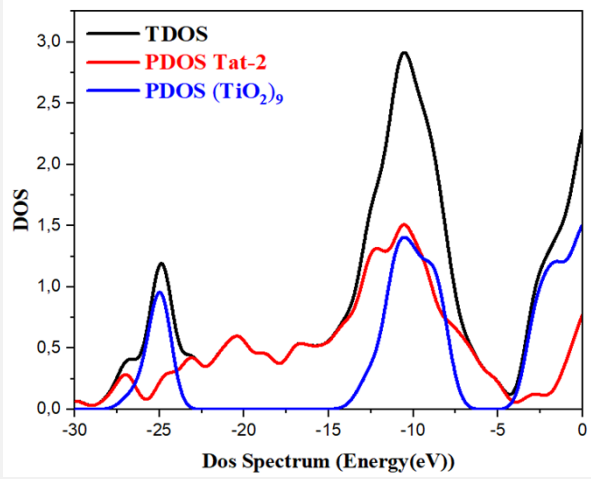
Dyes	E_{LUMO}	E_{CBM}	ΔG^0	λ_{total}
R_d	-2.804	-3.231	0.427	0.178
Tat-1	-3.141	-3.231	0.09	0.197
Tat-2	-3.246	-3.231	0.015	0.200
Tat-3	-3.000	-3.231	0.231	0.203
Tat-4	-3.230	-3.231	0.001	0.207
Tat-5	-3.158	-3.231	0.073	0.189
Tat-6	-3.353	-3.231	0.122	0.225

Table S5. The comparison for photovoltaic data of R_d between experiment and theory.

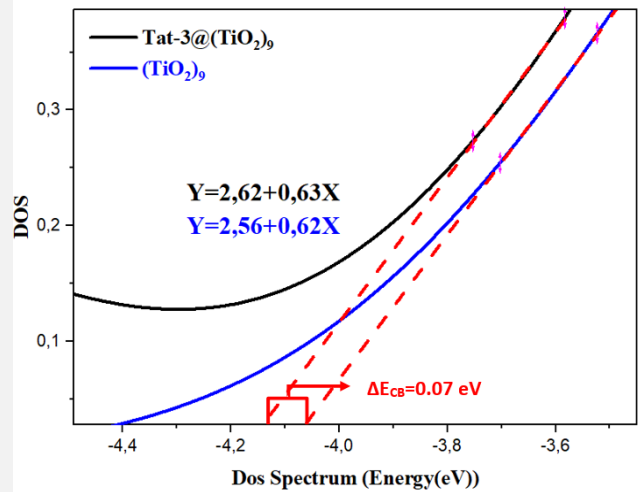
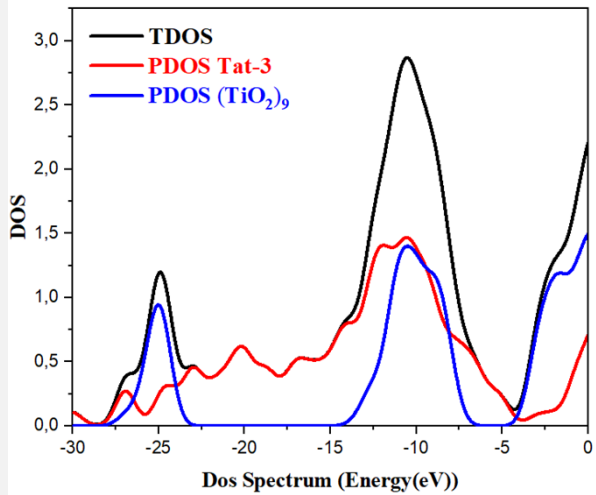
R	$J_{SC}(\text{mA cm}^{-2})$	$V_{OC}(\text{V})$	FF	PCE	Absorption (nm)
Experiment	19.74	0.957	0.708	13.4%[39]	519
Theory	19.21	0.838	0.865	13.92%	513.83
$ \Delta $	0.53	0.119	0.157	0.52%	5.17



(a)



(b)



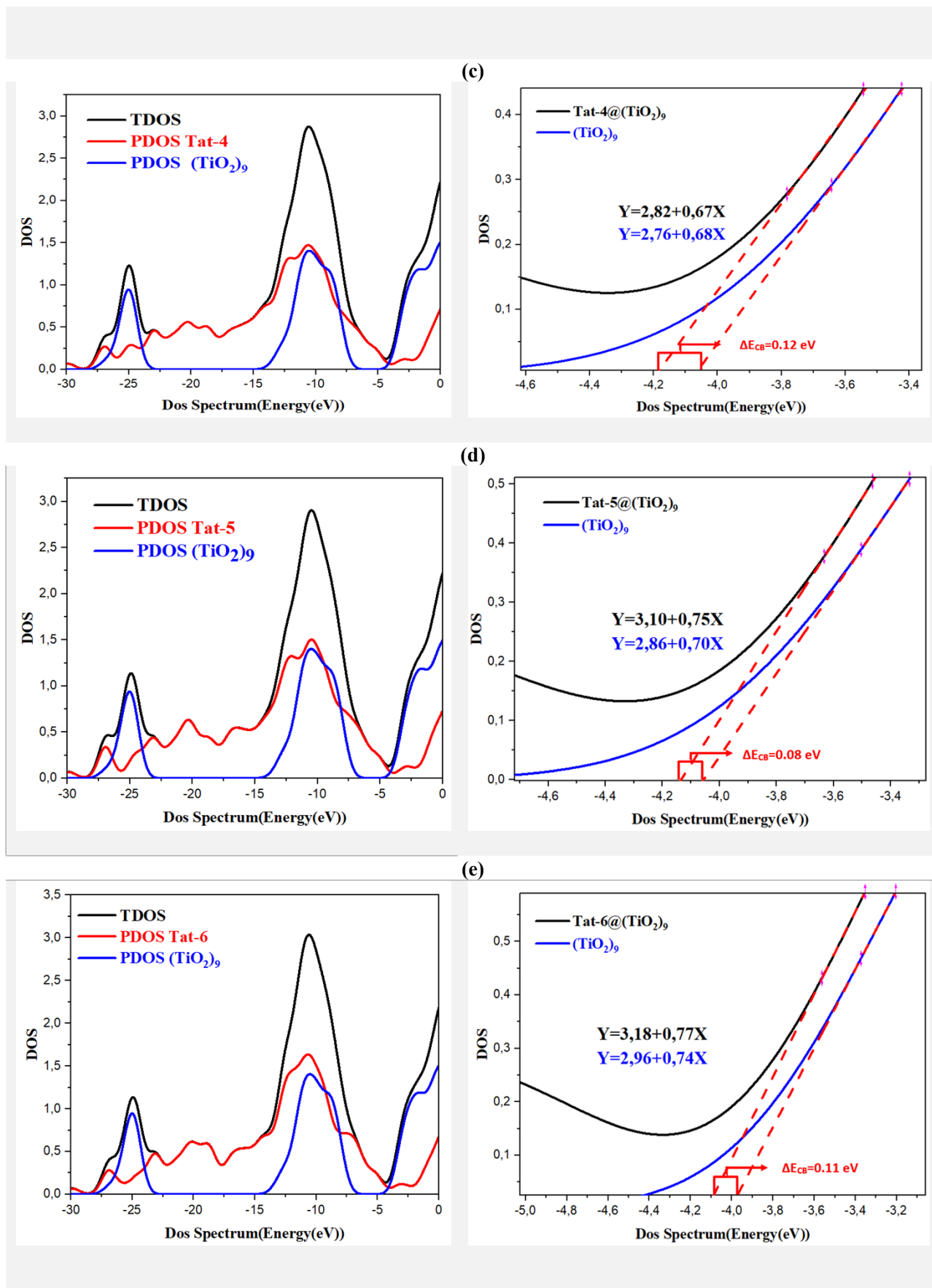


Figure S1. The calculated shift of conduction band (ΔE_{CB}) of simulated Dye@ $(TiO_2)_9$

composites. (a) presents the ΔE_{CB} of Tat-1; (b) presents the ΔE_{CB} of Tat-2; (c) presents the ΔE_{CB} of Tat-3; (d) presents the ΔE_{CB} of Tat-4; (e) presents the ΔE_{CB} of Tat-5; (f) presents the ΔE_{CB} of Tat-6.

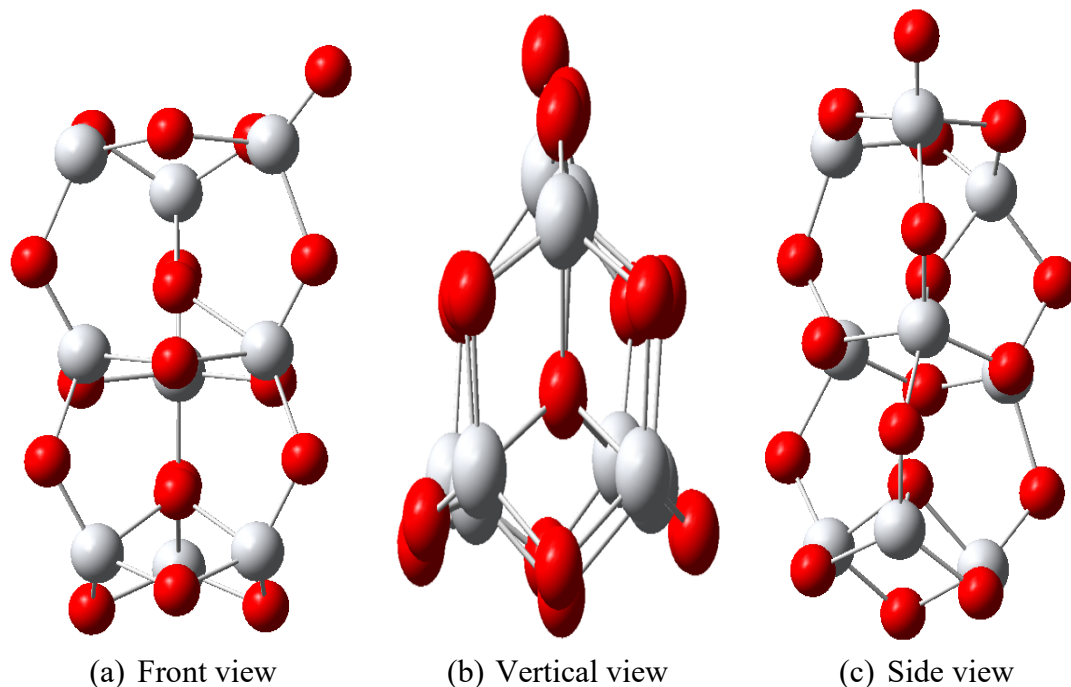


Figure S2. The geometry structure of optimized TiO_2 cluster. (a) The front view of the optimized structure. (b) The vertical view of the optimized structure. (c) The side view of the optimized structure.

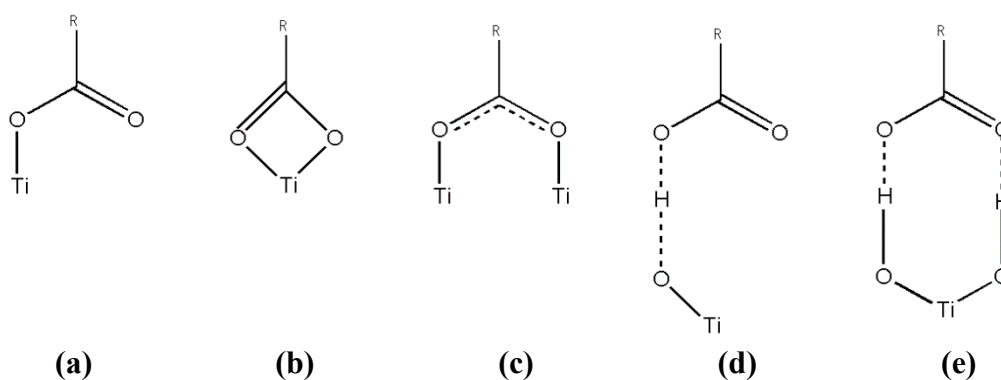
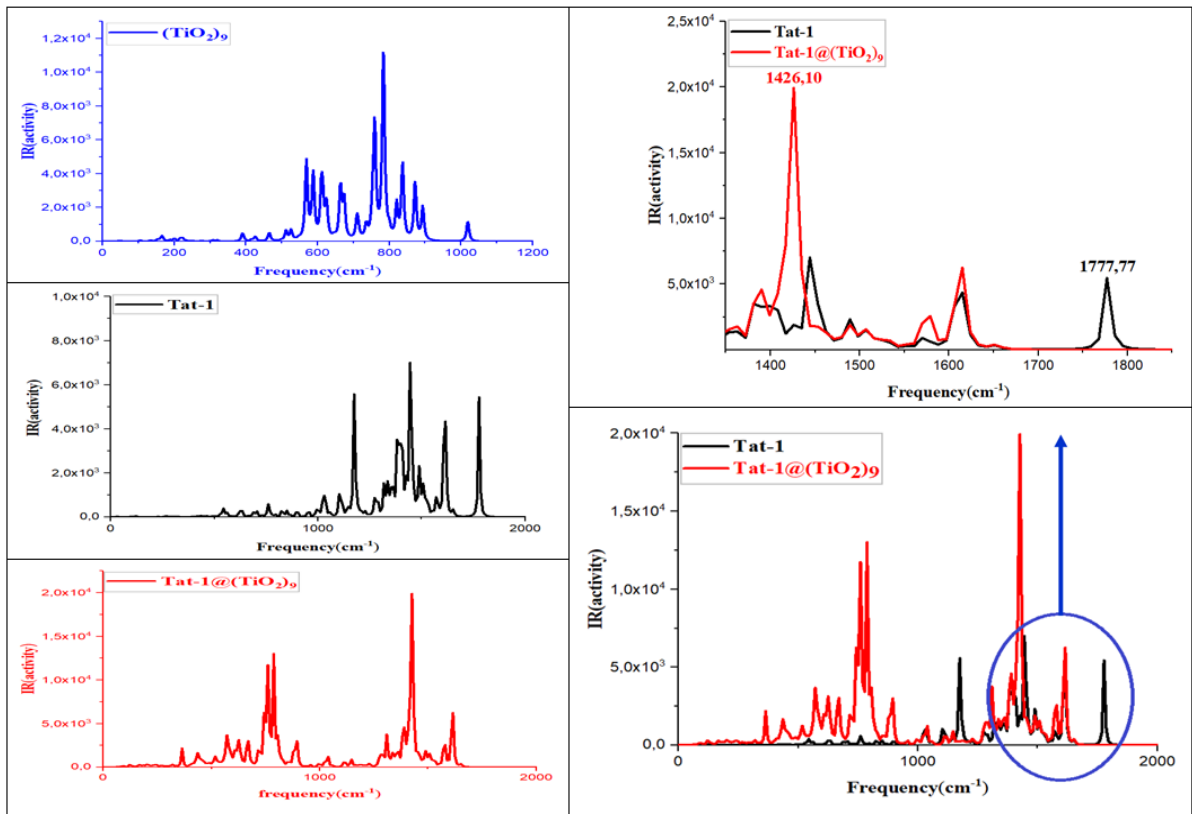
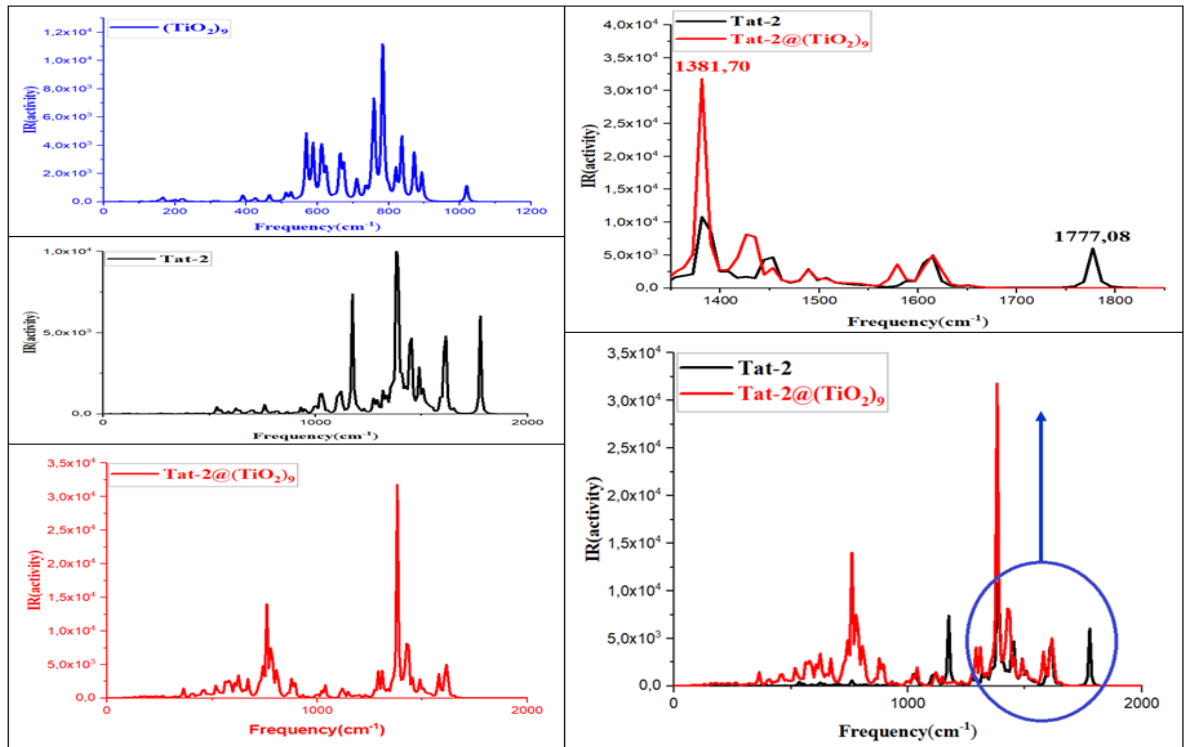


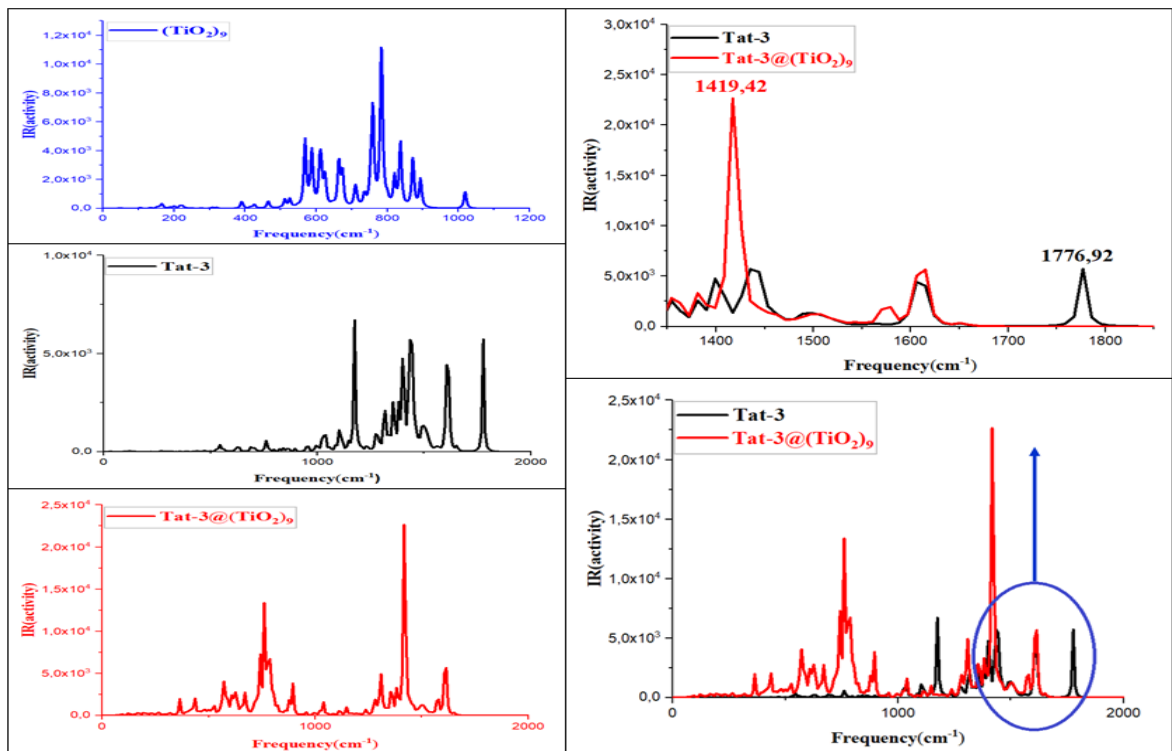
Figure S3. The connection model of carboxylic acid R-COOH group on TiO_2 clusters. (a) The connection model of monodentate ester. (b) The connection model of bidentate cheating (c) The connection model of bidentate bridging (d) The connection model of monodentate H-bonding (e) The connection model of bidentate H-bonding



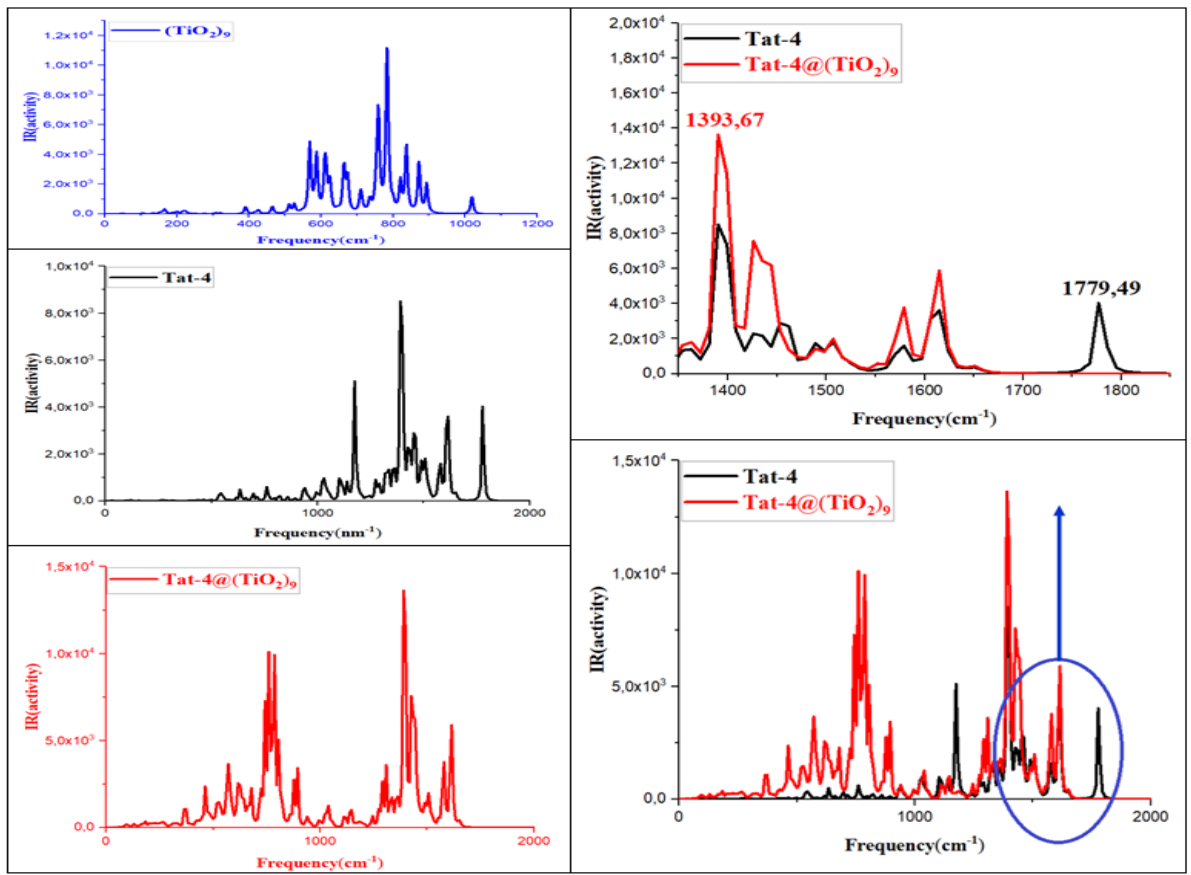
(a)



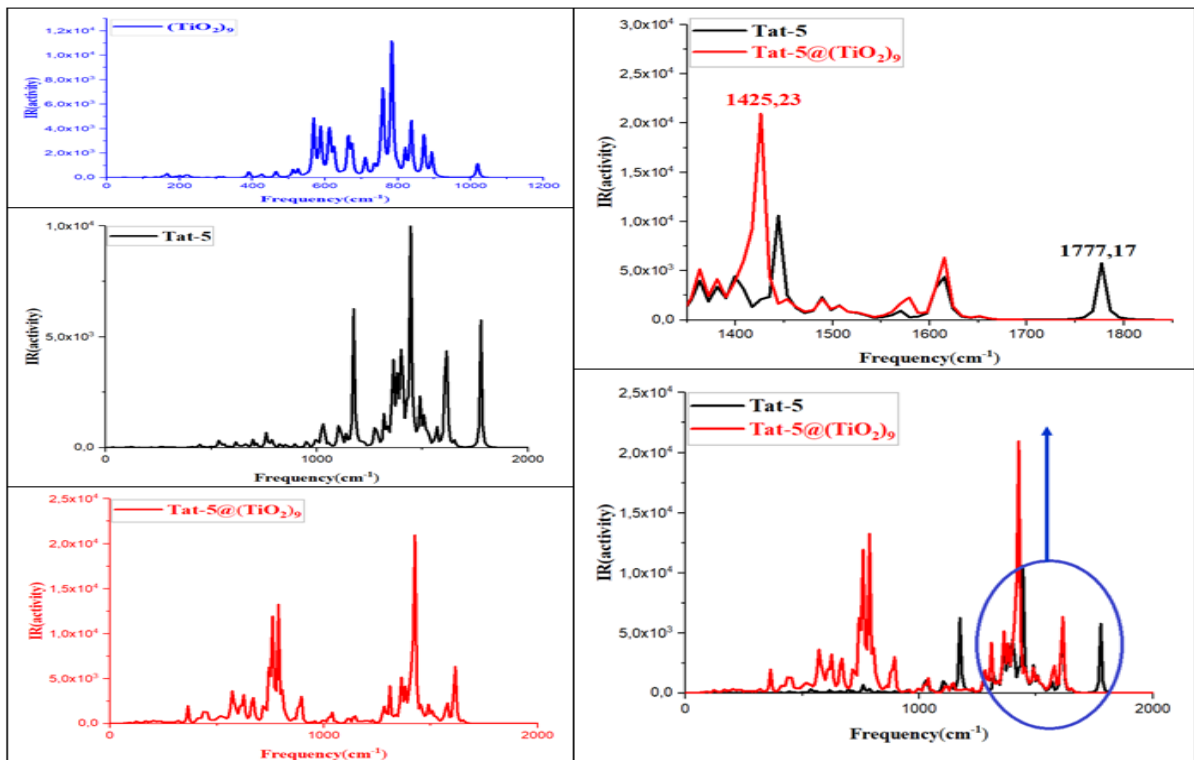
(b)



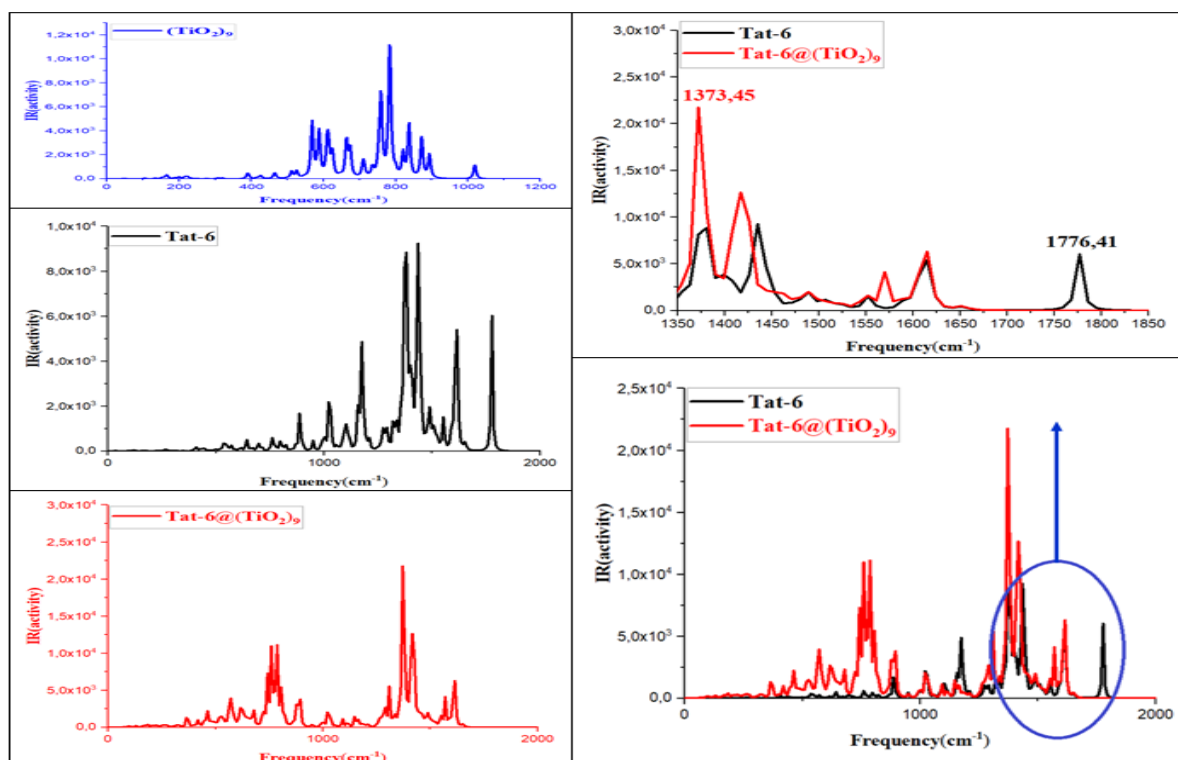
(c)



(d)



(e)



(f)

Figure S4. The FT-IR spectrum of isolated TiO_2 (in blue color), dye (in black color) Dye/ $(TiO_2)_9$ composites (in red color). (a) The black color presents the dye of Tat-1; The red color presents Tat-1@ $(TiO_2)_9$ composites; (b) The black color presents the dye of Tat-2; The red color presents Tat-2@ $(TiO_2)_9$ composites; (c) The black color presents dye of Tat-3; The red color presents Tat-3@ $(TiO_2)_9$ composites; (d) The black color presents dye of Tat-4; The red color presents Tat-4@ $(TiO_2)_9$ composites; (e) The black color presents dye of Tat-5; The red color presents Tat-5@ $(TiO_2)_9$ composites; (f) The black color presents dye of Tat-6; The red color presents Tat-6@ $(TiO_2)_9$ composites.

Reference

- [1] B.A. Gregg, Excitonic solar cells, *J. Phys. Chem. B.* 107 (2003) 4688–4698.
- [2] P. Politzer, F. Abu-Awwad, A comparative analysis of Hartree-Fock and Kohn-Sham orbital energies, (n.d.) 5.
- [3] J. Muscat, D. Newns, Chemisorption on metals, *Prog. Surf. Sci.* 9 (1978) 1–43.
- [4] P. Persson, M.J. Lundqvist, R. Ernstorfer, W. Goddard, F. Willig, Quantum chemical calculations of the influence of anchor-cum-spacer groups on femtosecond electron transfer times in dye-sensitized semiconductor nanocrystals, *J. Chem. Theory Comput.* 2 (2006) 441–451.
- [5] J. Calbo, M. Pastore, E. Mosconi, E. Ortí, F. De Angelis, Computational modeling of single-versus double-anchoring modes in di-branched organic sensitizers on TiO_2 surfaces: structural and electronic properties, *Phys. Chem. Chem. Phys.* 16 (2014) 4709–4719.

- [6] S. Belviso, E. Santoro, M. Penconi, S. Righetto, F. Tessore, Thioethyl porphyrazines: Attractive chromophores for second-order nonlinear optics and DSSCs, *J. Phys. Chem. C.* 123 (2019) 13074–13082.
- [7] X. Wang, Y. Li, P. Song, F. Ma, Y. Yang, Effect of graphene between photoanode and sensitizer on the intramolecular and intermolecular electron transfer process, *Phys. Chem. Chem. Phys.* 22 (2020) 6391–6400.
- [8] M. Li, L. Kou, L. Diao, Q. Zhang, Z. Li, Q. Wu, W. Lu, D. Pan, Z. Wei, Theoretical study of WS-9-based organic sensitizers for unusual Vis/NIR absorption and highly efficient dye-sensitized solar cells, *J. Phys. Chem. C.* 119 (2015) 9782–9790.
- [9] T. Le Bahers, T. Pauporté, G. Scalmani, C. Adamo, I. Ciofini, A TD-DFT investigation of ground and excited state properties in indoline dyes used for dye-sensitized solar cells, *Phys. Chem. Chem. Phys.* 11 (2009) 11276–11284.
- [10] P. Ren, C. Sun, Y. Shi, P. Song, Y. Yang, Y. Li, Global performance evaluation of solar cells using two models: from charge-transfer and recombination mechanisms to photoelectric properties, *J. Mater. Chem. C.* 7 (2019) 1934–1947.
- [11] T. Le Bahers, C. Adamo, I. Ciofini, A Qualitative Index of Spatial Extent in Charge-Transfer Excitations, *J. Chem. Theory Comput.* 7 (2011) 2498–2506. <https://doi.org/10.1021/ct200308m>.
- [12] C.A. Guido, P. Cortona, B. Mennucci, C. Adamo, On the Metric of Charge Transfer Molecular Excitations: A Simple Chemical Descriptor, *J. Chem. Theory Comput.* 9 (2013) 3118–3126. <https://doi.org/10.1021/ct400337e>.
- [13] F. Gao, C.-L. Yang, M.-S. Wang, X.-G. Ma, W.-W. Liu, Theoretical insight on hybrid nanocomposites of graphene quantum dot and carbazole–carbazole dyes as an efficient sensitizer of DSSC, *Spectrochim. Acta. A. Mol. Biomol. Spectrosc.* 216 (2019) 69–75. <https://doi.org/10.1016/j.saa.2019.02.107>.
- [14] T.-F. Lu, W. Li, F.-Q. Bai, R. Jia, J. Chen, H.-X. Zhang, Anionic ancillary ligands in cyclometalated Ru (II) complex sensitizers improve photovoltaic efficiency of dye-sensitized solar cells: insights from theoretical investigations, *J. Mater. Chem. A.* 5 (2017) 15567–15577.
- [15] M. Grätzel, Solar energy conversion by dye-sensitized photovoltaic cells, *Inorg. Chem.* 44 (2005) 6841–6851.
- [16] X. Liu, J. Han, H. Zhao, H. Yan, Y. Shi, M. Jin, C. Liu, D. Ding, Pressure dependence of excited-state charge-carrier dynamics in organolead tribromide perovskites, *Appl. Phys. Lett.* 112 (2018) 191903.
- [17] C. Yang, P. Song, R.M. El-Shishtawy, F. Ma, Y. Li, Photovoltaic performance and power conversion efficiency prediction of double fence porphyrins, *Phys. Chem. Chem. Phys.* 23 (2021) 27042–27058.
- [18] D. Zhao, R.M. Saputra, P. Song, Y. Yang, Y. Li, How graphene strengthened molecular photoelectric performance of solar cells: A photo current-voltage assessment, *Sol. Energy.* 213 (2021) 271–283. <https://doi.org/10.1016/j.solener.2020.11.034>.
- [19] X. Shi, Y. Yang, L. Wang, Y. Li, Introducing Asymmetry Induced by Benzene Substitution in a Rigid Fused π Spacer of D- π -A-Type Solar Cells: A Computational Investigation, *J. Phys. Chem. C.* 123 (2019) 4007–4021. <https://doi.org/10.1021/acs.jpcc.8b10963>.
- [20] M.K. Nazeeruddin, A. Kay, I. Rodicio, R. Humphry-Baker, E. Müller, P. Liska, N. Vlachopoulos, M. Grätzel, Conversion of light to electricity by cis-X2bis (2, 2'-bipyridyl-4, 4'-dicarboxylate) ruthenium (II) charge-transfer sensitizers (X= Cl-, Br-, I-, CN-, and SCN-) on nanocrystalline titanium dioxide electrodes, *J. Am. Chem. Soc.* 115 (1993) 6382–6390.
- [21] W. Zhang, L. Wang, L. Mao, J. Jiang, H. Ren, P. Heng, H. Ågren, J. Zhang, Computational protocol for precise prediction of dye-sensitized solar cell performance, *J. Phys. Chem. C.* 124 (2020) 3980–3987.
- [22] K. Prakash, A.Z. Alsaleh, P. Rath, A. Sharma, M. Sankar, F. D'Souza, Synthesis, Spectral, Electrochemical and Photovoltaic Studies of A3B Porphyrinic Dyes having Peripheral Donors, *ChemPhysChem.* 20 (2019) 2627–2634.
- [23] P. Heng, B. An, H. Ren, Y. Hu, X. Guo, L. Mao, L. Wang, J. Zhang, Influence of Different Molecular Design Strategies on Photovoltaic Properties of a Series of Triphenylamine-Based Organic Dyes for Dye-Sensitized Solar Cells: Insights from Theoretical Investigations, *J. Phys. Chem. C.* 124 (2020) 15036–15044.
- [24] D. Zhao, R.M. Saputra, P. Song, Y. Yang, F. Ma, Y. Li, Enhanced photoelectric and photocatalysis performances of quinacridone derivatives by forming D- π -A structure, *Sol. Energy.* 201 (2020) 872–883. <https://doi.org/10.1016/j.solener.2020.03.053>.

- [25] W. Ma, Y. Jiao, S. Meng, Predicting energy conversion efficiency of dye solar cells from first principles, *J. Phys. Chem. C*. 118 (2014) 16447–16457.
- [26] N.J. Cherepy, G.P. Smestad, M. Grätzel, J.Z. Zhang, Ultrafast electron injection: implications for a photoelectrochemical cell utilizing an anthocyanin dye-sensitized TiO₂ nanocrystalline electrode, *J. Phys. Chem. B*. 101 (1997) 9342–9351.
- [27] R. Marcus, Theory of electron-transfer reaction rates of solvated electrons, *J. Chem. Phys.* 43 (1965) 3477–3489.
- [28] P. Heng, L. Mao, X. Guo, L. Wang, J. Zhang, Accurate estimation of the photoelectric conversion efficiency of a series of anthracene-based organic dyes for dye-sensitized solar cells, *J. Mater. Chem. C*. 8 (2020) 2388–2399.
- [29] Z. Ning, Y. Fu, H. Tian, Improvement of dye-sensitized solar cells: what we know and what we need to know, *Energy Environ. Sci.* 3 (2010) 1170. <https://doi.org/10.1039/c003841e>.
- [30] T. Marinado, K. Nonomura, J. Nissfolk, Martin.K. Karlsson, D.P. Hagberg, L. Sun, S. Mori, A. Hagfeldt, How the Nature of Triphenylamine-Polyene Dyes in Dye-Sensitized Solar Cells Affects the Open-Circuit Voltage and Electron Lifetimes, *Langmuir*. 26 (2010) 2592–2598. <https://doi.org/10.1021/la902897z>.
- [31] T. Marinado, D.P. Hagberg, M. Hedlund, T. Edvinsson, E.M.J. Johansson, G. Boschloo, H. Rensmo, T. Brinck, L. Sun, A. Hagfeldt, Rhodaninedyes for dye-sensitized solar cells : spectroscopy, energy levels and photovoltaic performance, *Phys Chem Chem Phys*. 11 (2009) 133–141. <https://doi.org/10.1039/B812154K>.
- [32] E. Ronca, M. Pastore, L. Belpassi, F. Tarantelli, F. De Angelis, Influence of the dye molecular structure on the TiO₂ conduction band in dye-sensitized solar cells: disentangling charge transfer and electrostatic effects, *Energy Environ. Sci.* 6 (2013) 183–193.
- [33] S. Yusuf, A. Azzahari, V. Selvanathan, R. Yahya, M. Careem, A.K. Arof, Improvement of N-phthaloylchitosan based gel polymer electrolyte in dye-sensitized solar cells using a binary salt system, *Carbohydr. Polym.* 157 (2017) 938–944.
- [34] W. Li, J. Wang, J. Chen, F.-Q. Bai, H.-X. Zhang, Theoretical investigation and design of high-efficiency dithiafulvenyl-based sensitizers for dye-sensitized solar cells: the impacts of elongating π -spacers and rigidifying dithiophene, *Phys. Chem. Chem. Phys.* 16 (2014) 9458–9468.
- [35] P. Li, Y. Cui, C. Song, H. Zhang, A systematic study of phenoxazine-based organic sensitizers for solar cells, *Dyes Pigments*. 137 (2017) 12–23.
- [36] U. Sultan, F. Ahmadloo, G. Cha, B. Gökcan, S. Hejazi, J.-E. Yoo, N.T. Nguyen, M. Altomare, P. Schmuki, M.S. Killian, A High-Field Anodic NiO Nanosponge with Tunable Thickness for Application in p-Type Dye-Sensitized Solar Cells, *ACS Appl. Energy Mater.* 3 (2020) 7865–7872.
- [37] J.K. Roy, S. Kar, J. Leszczynski, Revealing the photophysical mechanism of N, N'-Diphenyl-aniline based sensitizers with the D–D– π –A framework: theoretical insights, *ACS Sustain. Chem. Eng.* 8 (2020) 13328–13341.
- [38] I.-Y. Jeon, H.M. Kim, D.H. Kweon, S.-M. Jung, J.-M. Seo, S.-H. Shin, I.T. Choi, Y.K. Eom, S.H. Kang, H.K. Kim, Metalloid tellurium-doped graphene nanoplatelets as ultimately stable electrocatalysts for cobalt reduction reaction in dye-sensitized solar cells, *Nano Energy*. 30 (2016) 867–876.
- [39] L. Zhang, X. Yang, S. Li, Z. Yu, A. Hagfeldt, L. Sun, Electron-Withdrawing Anchor Group of Sensitizer for Dye-Sensitized Solar Cells, Cyanoacrylic Acid, or Benzoic Acid?, *Sol. RRL*. 4 (2020) 1900436. <https://doi.org/10.1002/solr.201900436>.